Stochastic bivariate time series models of waves in the North Sea and their application in simulation-based design

Endre Sandvik[a,*], Ole J.J. Lønnum[a], Bjørn E. Asbjørnslett[a]

[a] *Department of Marine Technology, Norwegian University of Science and Technology (NTNU), NO-7491 Trondheim, Norway*

Abstract

In this paper, we present and evaluate three long-term wave models for application in simulation-based design of ships and marine structures. Designers and researchers often rely on historical weather data as a source for ocean area characteristics based on hindcast datasets or in-situ measurements. The limited access and size of historical datasets reduces repeatability of simulations and analyses, making it difficult to assess the sampling variability of performance and loads on marine vessels and structures. Markov, VAR and VARMA wave models, producing independent long-term time series of significant wave height (H_s) and spectral peak period (T_p), is presented as possible solutions to this problem. The models are tested and compared by addressing how the models affect interpretation of design concepts and the ability to replicate statistical and physical characteristics of the wave process. Our results show that the VAR and VARMA models perform sufficiently in describing design performance, but does not capture the physical process fully. The Markov model is found to perform worst of the tested models in the applied tests, especially for measures covering several consecutive sea states.

Keywords: Significant wave height, spectral peak period, stochastic time series modelling, simulation-based design

1. Introduction

Exposure to weather is a key challenge for engineers and designers working on marine technology projects and activities. Waves, wind and current affect the ability to perform marine operations and increases required propulsion power of ships, the extent of which is valuable knowledge during design. Virtual testing procedures, incorporating the effects of the surrounding environment, has in recent years been developed to improve our understanding of the scenarios ships and ocean structures are likely to face and the corresponding performance. The present work addresses the long-term modelling of waves and the impact alternative formulations has on our interpretation of ship added resistance and operability.

Simulation-based approaches for studying maritime systems and entities has existed for some time. In the IDEAS project benchmarking of ship design concepts using hindcast weather data and discrete-event simulation (DES) is performed to enhance power requirement estimates [13]. HOLISHIP is an international research project working towards the development of a simulation-based integrated decision support system to cover all aspects of ship design [21]. The ViProMa project (Vitrual Prototyping of Maritime Systems and Operations) is a knowledge-building project using co-simulation for prototyping in the design process [29]. Bergström et al. [3] presents a simulation-based approach for assessing Arctic transport systems and ships in ice infested waters, providing a discussion on model fidelity and sources of uncertainty in [4]. Vernengo and Rizzuto [37] presents a ship synthesis model for exploration of the design space for compressed natural gas carriers, and illustrates its applicability for

*Corresponding author
Email address: `endre.sandvik@ntnu.no` (Endre Sandvik)
URL: `https://www.ntnu.no/ansatte/endre.sandvik` (Endre Sandvik)

power and capacity variations in [36]. Design and planning of operations and fleet sizing problems often apply stochastic models for representation of weather-induced delays, see e.g. [28] and [19].

For many years, *Global Wave Statistics* was the primary source of wave data for design of ships [17]. The data was collected by visual observations from ships in service all over the world since 1949, and is presented as scatter diagrams of significant wave height (H_s) and mean zero-crossing period (T_z) sorted according to propagation direction and season. Alternative sources of data has been established based on in-situ measurements, numerical wave prediction models and satellite data. Instrumentally recorded wave measurements is considered superior to model derived data, but is expensive and time consuming to collect. Hence, the availability of sufficiently long in-situ time series is limited. Hindcast numerical models has been applied to assess and estimate the global metocean wave climate. The WAM model is applied by many commercial wave databases and has been subject to extensive testing and improvement in recent years [38] [20]. Bitner-Gregersen and Guedes Soares [6] addresses the uncertainty of the average wave steepness by comparing three hindcast wave databases and data given in *Global Wave Statistics*. Campos and Guedes Soares [8] compares and assess three wave hindcasts in the North Atlantic Ocean. These studies revealed important differences in terms of extreme conditions, and that the magnitude of the differences is site-specific. For non-extreme conditions, the hindcasts produce very similar values overall. Vanem [35] presents an extensive review of stochastic long-term wave models, focussing primarily on estimation of extreme sea states but also covering literature on modelling of time and space dependent variables in general. Monbet et al. [22] provides a review over stochastic time series models for wind and sea states, stating that the context of use is important for determining whether a model is suitable.

The scope of this article is to present and compare stochastic bivariate wave models for producing synthetic long-term time series for application in simulation-based design of marine systems. Previous research has to a large extent focused on the fundamental statistical properties of models, as well as for prediction and filling missing time series values. The present paper contributes by testing and comparing the models in view of their effect on important marine engineering parameters in a design context. We have two main objectives in this paper: First, to present three long-term wave models by which bivariate synthetic time series of H_s and T_p can be generated. Second, present a comparison to hindcast data for relevant measures in simulation-based design to demonstrate the practical implications of their formulation.

The paper is structured in seven sections. In the following section, we illustrate the steps of stochastic wave model development and the connection to simulation and design theory. Next, we present three candidate wave models in terms of their mathematical formulation and assumptions. In Section 4, a presentation of the testing and benchmarking scheme for assessing wave model application in simulation-based design is given. Sections 5 and 6 presents the results from the study and gives a discussion of the practical implications, respectively. Finally, the last section lists the main findings and conclusions.

2. Wave models and impact on design interpretation

2.1. Simulation in marine design

Design of ships and marine structures includes analyses to determine the influence of ocean environment on safety and performance. Loads and motions excited by the occurring waves, wind, and current must be considered to ensure safety of personnel and the asset as well as profitability margins. In a design context, simulation is applied as a tool for mapping between the design space and performance space. This mapping relies on what is referred to as interpretive knowledge, meaning the knowledge of how a given set of design variables materialize to a set of performance quantities. Figure 1 shows how our interpretation of a ship design concept is linked to the assumptions and modelling approach for long-term wave models. Based on the system theories of the long-term wave process, a conceptual model is formulated in the form of a mathematical/logical/graphical representation of the system, represented here as a decomposition of the yearly season variation and the stochastic process of wave formation in the short-term horizon. Specifying further, we assume that the seasonal effects can be obtained using Fourier and statistical analysis, and the short-term contribution can be modelled as a Markov process. Statistical analysis is then performed using the long-term dataset of real waves, giving us the complete model.

The model can then be applied in a simulation framework where we replicate the environmental impact on ships during operation. This process allow us to observe how the ship behave in terms of relevant measures for e.g. safety, operational performance, fuel consumption. As mentioned above, simulation is applied for mapping between the design and performance space. We convert our representation of form (synthesis) to a measure of function (semantics). Figure 1 shows how the modelling choices we make during model development affect this relation.

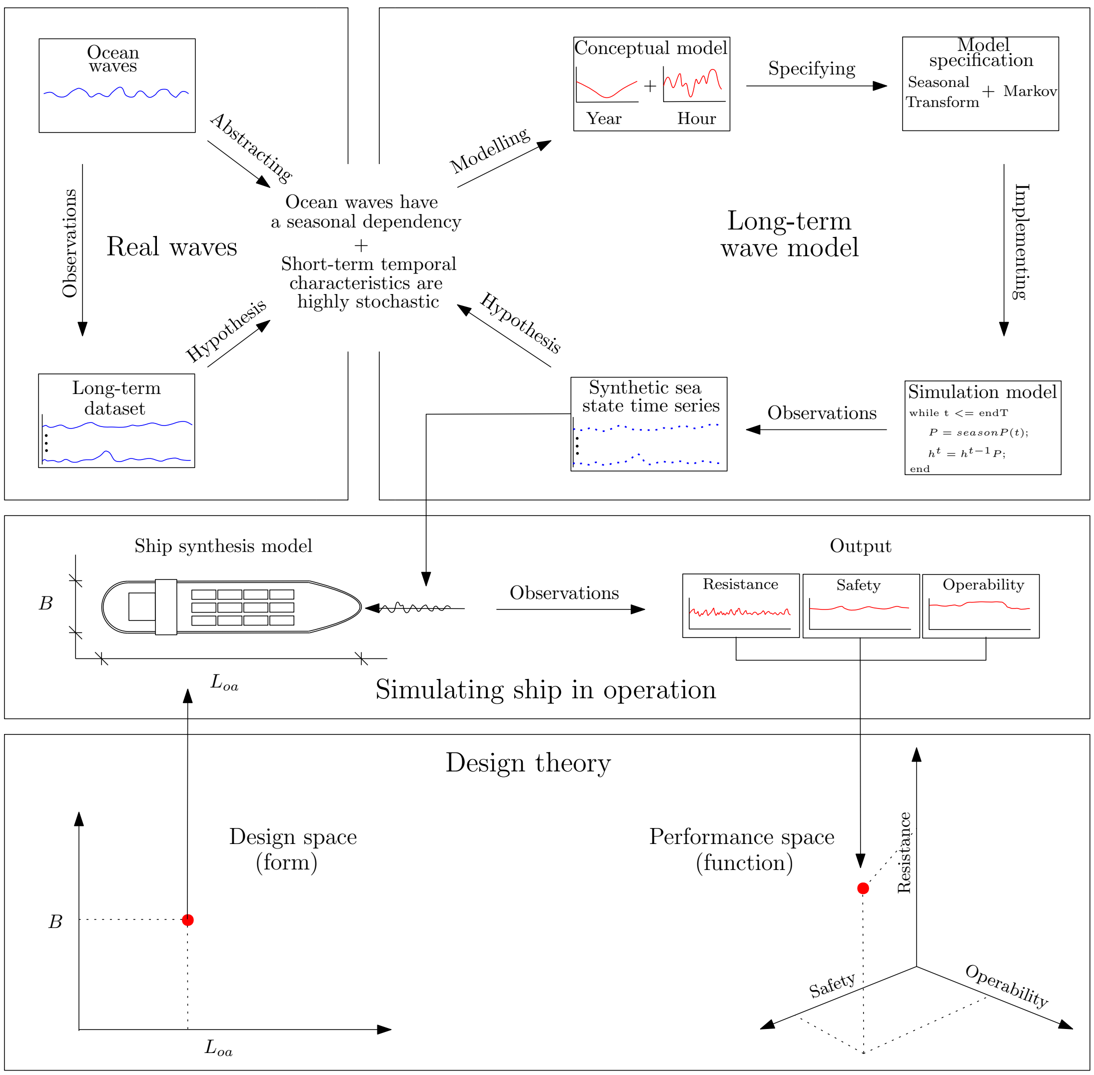

Figure 1: The stages of wave modelling and its connection to ship performance evaluation during design, exemplified by Markov model. (Top part of figure adapted and modified from [27])

The interpretation of a ship design concept should not be a function of the chosen wave model formulation, but rather the characteristics of the actual wave environment occurring at the site or route of operation. However, differences may develop as a consequence of model abstraction and simulation model specification. The corresponding impact on the design parameters varies with the parameter dependency towards the simulated wave environment. For example, marine operations require weather windows of a sufficient length and sea state intensity, implying sensitivity towards the occurring sea state levels and persistence.

Fuel consumption for a ship in a seaway, as a function of wave added resistance, is dependent on the occurring sea state parameters, permitting evaluation using wave parameter distributions. These differences in dependencies towards the generated synthetic time series is the reason for choosing the test scheme presented in Section 4, and forms the basis for discussing model applicability in Section 6.

2.2. The stochastic process of waves

The wave generation process and the dynamics of water surface behaviour follows the laws of physics and is generally well understood. However, waves and sea systems are influenced by countless factors and parameters, making deterministic analysis impossible due to the system complexity. Hence, waves are modelled using probabilistic models [35]. This implies that design parameters dependent on wave intensity and occurrence are subject to uncertainty. Bitner-Gregersen et al. [5] addresses uncertainties in wind and wave description in the context of engineering applications, dividing this uncertainty in two groups: aleatory and epistemic uncertainty. Aleatory uncertainty is the inherent variability of a given parameter due to the process of which it is generated. Epistemic uncertainty is related to the lack of knowledge for describing the parameter, and can subsequently be reduced by acquiring more data. For design of ships and marine structures, we are interested in the variability of our estimates occurring as a consequence of the environment of which it operates, i.e. aleatory uncertainty. Efforts are generally made to reduce epistemic uncertainty to a minimum, as it obscures the vision of how a system performs. Variability of design performance using simulation is normally assessed by repeating simulations. This process provides confidence bounds for the performance resulting from the inherent variability of the system environment. However, especially considering long-term simulations, such analyses require large sets of accessible data for constructing equivalent simulation scenarios. This necessitates synthetic time series from a scenario generator, which is the role of the stochastic wave models in the present work.

3. Bivariate long-term wave models

3.1. Hindcast data

In the present work we apply hindcast data from a single location in the North Sea positioned 56°31'N, 3°14'E shown in Figure 2. The dataset is provided by the Norwegian Meteorological Institute from the hindcast archive NORA10 (NOrwegian ReAnalysis 10 km), see [26]. Time series of H_s and T_p with a temporal resolution of 3 h between 1958 and 2016 is provided.

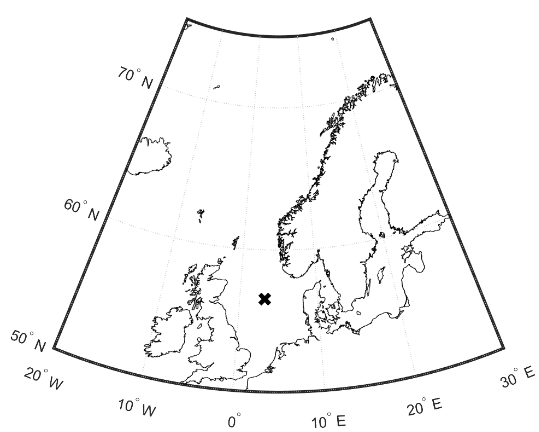

Figure 2: Location for wave data in the North Sea

3.2. Data transformation

Transformation of the hindcast data is applied to produce a stationary set of residuals W for which the models can be fitted. The VAR and VARMA models (see Section 3.4) both assume stationary time series behaviour. The hindcast data have a yearly statistical periodicity due to the meteorological annual cycle, which must be removed before the models can be fitted.

3.2.1. Rosenblatt transform

The common method for creating approximately Gaussian time series is to apply a from of logarithmic transformation, e.g. the Box-Cox transformation [7]. In the present work, we apply a log-normal Rosenblatt transformation to model the joint behaviour of H_s and T_p (see [24]). It is based on the Conditional Modelling Approach (CMA) given in DNV GL [11]. The joint density function $f_{H_sT_p}(h,t)$ is described using a marginal distribution of H_s and a conditional distribution of $T_p|H_s$. Therefore, the marginal distribution of H_s is assumed to follow a lognormal distribution given by

$$f_{H_s}(h) = \frac{1}{\sigma_h h\sqrt{2\pi}} \exp\left\{-\frac{(\ln h - \mu_h)}{2\sigma_h^2}\right\} \tag{1}$$

where μ_h and σ_h are distribution parameters estimated from the hindcast data. The conditional distribution of $T_p|H_s$ is estimated as

$$f_{T_p|H_s}(t|h) = \frac{1}{\sigma_{t|h} t\sqrt{2\pi}} \exp\left\{-\frac{(\ln t - \mu_{t|h})}{2\sigma^2}\right\} \tag{2}$$

where $\mu_{t|h}$ and $\sigma_{t|h}$ are represented by functions

$$\begin{aligned} \mu_{t|h} &= E\left[\ln T_p\right] = a_0 + a_1 h^{a_2} \\ \sigma_{t|h} &= std\left[\ln T_p\right] = b_0 + b_1 \exp\left(b_2 h\right) \end{aligned} \tag{3}$$

a_{0-2} and b_{0-2} are curve fitting coefficients. Transformation to Gaussian U-space is then given by

$$\begin{aligned} u_h &= \Phi^{-1}\left(F_{H_s}(h)\right) \\ u_t &= \Phi^{-1}\left(F_{T_p|H_s}(t)\right) \end{aligned} \tag{4}$$

DNV GL [11] recommends fitting a 3-parameter Weibull distribution to the marginal distribution of H_s. Figure 3 shows the comparison of 3-parameter Weibull and lognormal fit for the H_s marginal distribution. Both show a reasonable fit to the hindcast data. The 3-parameter Weibull distribution is recognized by its location parameter which introduces a lower limit for the distribution (0.422 in this case). The benefit of the location parameter is that a better fit can be achieved for the distribution tail, i.e. the high H_s range. The lognormal distribution is defined for all positive H_s values, but gives a wider tail than the Weibull distribution. This difference implies that the lognormal distribution is more susceptible for generating extreme sea state events. However, as seen in the residual distribution plot in Figure 3, the lognormal distribution residuals has a more symmetric distribution. Hence, it is more suited for implementation in the VAR and VARMA models which utilizes a white noise error component, see Section 3.4.1. The Box-Cox log-transformation results in an equally symmetric residual distribution, but is rejected in the present work as the corresponding joint distribution of H_s and T_p is found to be poorly replicated.

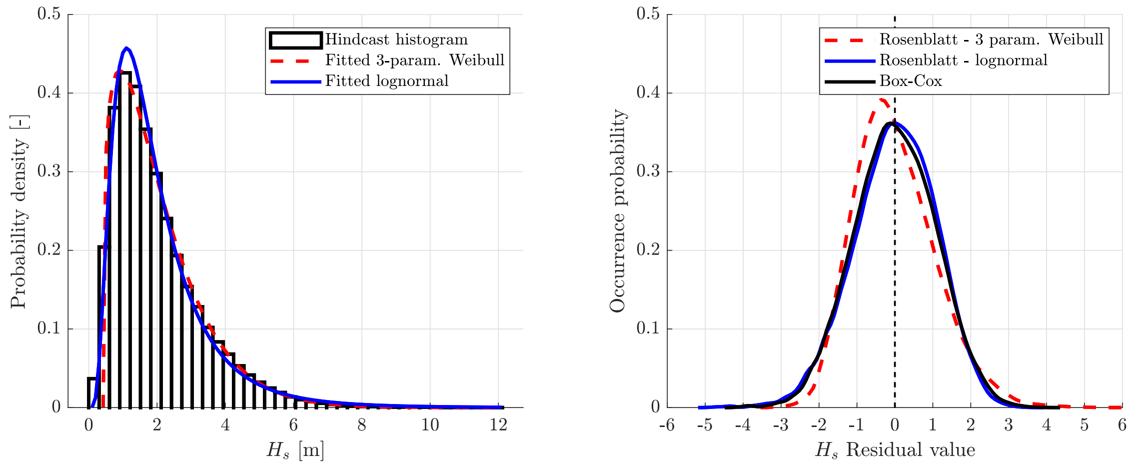

Figure 3: Distribution fit for hindcast wave data (left) and residual distribution plot (right)

3.2.2. Multivariate seasonal transform

To remove the yearly meteorological periodicity of u_h and u_t, the seasonal transformation given in [32] is applied. First, it is assumed that the u_h and u_t series can be decomposed as

$$Y_t = M_t + \Sigma_t W_t \tag{5}$$

where Y_t is a vector of the bivariate u_h and u_t data, M_t is the mean vector and Σ_t the standard deviation matrix. Σ_t is taken as the square root of the covariance matrix. M_t and Σ_t are deterministic periodic functions with period equal to one year. The seasonal pattern coefficients in Σ_t and M_t is estimated by first sorting the terms of Y_t according to the triple notation $Y_n(j, k, \tau_k)$. The indexes are given by the number of years J such that $j = 1, \ldots, J$, m specifies the month $m = 1, \ldots, 12$, and $k = 1, \ldots, k_m$, where k_m is the number of observations in month m. The time series of monthly mean and covariance can then be approximated as

$$M_n(j, m) = \frac{1}{k_m} \sum_{k=1}^{k_m} Y_n(j, m, \tau_k) \quad n = 1, \ldots, N \tag{6}$$

$$\begin{aligned} S_{nl}(j, m) = \frac{1}{k_m} \sum_{k=1}^{k_m} \{ &[Y_n(j, m, \tau_k) - M_{3,n}(j, m)] \\ &\times [Y_l(j, m, \tau_k) - M_{3,n}(j, m)] \} \end{aligned} \tag{7}$$

where τ_k is the observation index of sample points in month m in year j. The mean and covariance of the seasonal patterns can then be estimated as

$$\tilde{M}_n(m) = \frac{1}{J} \sum_{j=1}^{J} M_{\nu n}(j, m) \tag{8}$$

$$\tilde{S}_{nl}(m) = \frac{1}{J} \sum_{j=1}^{J} S_{\nu nl}(j, m) \tag{9}$$

Stefanakos and Athanassoulis [31, 30] states that the periodic extensions of $\tilde{M}_n(m)$ and $\tilde{S}_{nl}(m)$ are good estimates for M_{nt} and Σ_{nlt} respectively. Fourier series were fitted to $\tilde{M}_n(m)$ and $\tilde{S}_{nl}(m)$ to obtain M_{nt} and Σ_{nlt} estimates. The residual component W_t is then found as

$$W_t = \frac{Y_t - M_t}{\Sigma_t} \tag{10}$$

As an alternative, Guedes Soares and Cunha [15] states that transformation which disregards variance yields better results for some metocean series

$$W_t = Y_t - M_t \tag{11}$$

The Markov and VAR model were fitted to data transformed using the transform in Equation 11. For the VARMA model, full seasonal transform, i.e. including both mean and standard deviation as given in Equation 10 was applied.

3.2.3. Seasonal transform for Markov model

The Markov model does not need data that fulfil the Gaussian assumption, but require stationary distributions to generate the transition matrix **P** . In addition, the bivariate behaviour is modelled using a coupling matrix (see Section 3.3) which does not require stationarity nor Gaussian behaviour of T_p. Hence, H_s was subject to seasonal transform to obtain stationarity.

3.3. Markov chains

Finite-state space Markov chains are discrete stochastic processes which satisfies the Markov property. This property, often referred to as the memoryless property, is the assumption that the future variable state is only dependent on the current state. The discrete state space is given by $\Omega = \{1, 2, 3, \ldots, n\}$. Assuming that H_t is a random variable representing the state of H_s at time t, the Markov property then allow us to formulate the transition probability between state i and j as

$$p_{ij} = P(H_{t+1} = j | H_t = i) \tag{12}$$

The transition between states is governed by a transition matrix **P** stating the probabilities of transition between the current and all other states contained in the finite-state set.

$$\mathbf{P} = \begin{bmatrix} p_{11} & p_{12} & \cdots & p_{1n} \\ p_{21} & p_{22} & \cdots & p_{2n} \\ \vdots & \vdots & \ddots & \vdots \\ p_{n1} & p_{n2} & \cdots & p_{nn} \end{bmatrix} \tag{13}$$

To compute the transition probabilities, Anastasiou and Tsekos [2] applies a maximum likelihood estimator for the expressed as

$$\hat{p}_{ij} = \frac{N^h_{ij}}{N^h_i} \tag{14}$$

Where N^h_{ij} is the number of observed transitions from state i to state j, and N^h_i is the total number of occurrences of state i in the sequence. To obtain a bivariate model of H_s and T_p, we need to couple the occurrence of H_s and T_p states. There are several possible approaches to achieve this coupling, see [16]. For this model, we formulated a coupling matrix **C** given by

$$\mathbf{C} = \begin{bmatrix} c_{11} & c_{12} & \cdots & c_{1N_{tp}} \\ c_{21} & c_{22} & \cdots & c_{2N_{tp}} \\ \vdots & \vdots & \ddots & \vdots \\ c_{N_{hs}1} & c_{N_{hs}2} & \cdots & c_{N_{hs}N_{tp}} \end{bmatrix} \tag{15}$$

where N_{h_s} and N_{t_p} are the number of unique values in the model model for H_s and T_p, respectively. c_{ij} states the probability of T_p being in state j while H_s is in state i. The maximum likelihood estimator for c_{ij} is given by [2].

$$\hat{c}_{ij} = \frac{N_{ij}^{t,h}}{N_i^h} \tag{16}$$

The initiation of the model is done by sampling an initial condition W_0 from the W_t distribution. Calculation of of the succeeding values is done by

$$W_t = P(W_{t-1}) \tag{17}$$

Utilizing Equation 11, the back-transform to retrieve the corresponding $H_{s,t}$ value is expressed as

$$H_{s,t} = M_t + W_t \tag{18}$$

Finally, the corresponding T_p value is obtained using the the coupling matrix in Equation 15

$$T_{p,t} = C(H_{s,t}) \tag{19}$$

3.4. Autoregressive and moving-average models

3.4.1. Univariate AR, MA and ARMA models

The univariate $AR(p)$ model assumes that the next step is linearly dependent on the past p values and a random term. This is expressed on the form

$$W_t = c + \sum_{i=1}^{p} \phi_i W_{t-i} + \epsilon_t \tag{20}$$

where ϕ_i are the AR parameters, c is a constant ϵ_t is white noise. The univariate moving average model $MA(q)$ is expressed as

$$W_t = \epsilon_t + \sum_{i=1}^{q} \theta_i \epsilon_{t-i} \tag{21}$$

where q is the number of lags, θ_i are the MA parameters and ϵ_t is white noise. Univariate $ARMA(p,q)$ model is simply the composition of $AR(p)$ and $MA(q)$ models, expressed as:

$$W_t = c + \epsilon_t + \sum_{i=1}^{p} \phi_i W_{t-i} + \sum_{i=1}^{q} \theta_i \epsilon_{t-i} \tag{22}$$

3.5. Bivariate VAR and VARMA models

Extension of AR to the multivariate case is often referred to as vector AR or VAR. For the bivariate case, considering evolution of residuals W_t^H and W_t^T, we express the VAR model as

$$\begin{bmatrix} W_t^H \\ W_t^T \end{bmatrix} = \begin{bmatrix} c^H \\ c^T \end{bmatrix} + \sum_{i=1}^{p} \begin{bmatrix} \phi_i^{HH} & \phi_i^{HT} \\ \phi_i^{TH} & \phi_i^{TT} \end{bmatrix} \begin{bmatrix} W_{t-i}^H \\ W_{t-1}^T \end{bmatrix} + \begin{bmatrix} \epsilon_t^H \\ \epsilon_t^T \end{bmatrix} \tag{23}$$

Extension of $ARMA$ to the multivariate case is performed in the same manner as for the VAR model. For the bivariate case, considering evolution of residual components W_t^H and W_t^T, we express the $VARMA$ model as

$$
\begin{aligned}
\begin{bmatrix} W_t^H \\ W_t^T \end{bmatrix} = \begin{bmatrix} c^H + \epsilon_t^H \\ c^T + \epsilon_t^T \end{bmatrix} + \sum_{i=1}^{p} \begin{bmatrix} \phi_i^{HH} & \phi_i^{HT} \\ \phi_i^{TH} & \phi_i^{TT} \end{bmatrix} \begin{bmatrix} W_{t-i}^H \\ W_{t-i}^H \end{bmatrix} \\
+ \sum_{i=1}^{q} \begin{bmatrix} \theta_i^{HH} & \theta_i^{HT} \\ \theta_i^{TH} & \theta_i^{TT} \end{bmatrix} \begin{bmatrix} \epsilon_{t-i}^H \\ \epsilon_{t-i}^T \end{bmatrix}
\end{aligned} \tag{24}
$$

Utilizing equation 10, the reverse seasonal transformation of the residuals W_t^H and W_t^T for the VAR and VARMA model is expressed as

$$
\begin{bmatrix} u_t^H \\ u_t^T \end{bmatrix} = \begin{bmatrix} M_t^H \\ M_t^T \end{bmatrix} + \begin{bmatrix} \sigma_{u^H} & \sigma_{u^H u^T} \\ \sigma_{u^T u^H} & \sigma_{u^T} \end{bmatrix} \begin{bmatrix} W_t^H \\ W_t^T \end{bmatrix} \tag{25}
$$

Finally, reverse Rosenblatt transformation is applied to obtain corresponding H_s and T_p values. This is done by reversing Equation 4

$$
\begin{aligned}
H_{s,t} &= F_{H_s}^{-1}\left(\Phi(u_t^H)\right) \\
T_{p,t} &= F_{T_p|H_s}^{-1}\left(\Phi(u_t^T)\right)
\end{aligned} \tag{26}
$$

3.6. Parameter fitting

For the Markov chain model, the finite-state space size, i.e. the dimensions of matrices **P** and **C**, is important as it describes both the range and discretization of occurring values. The adopted approach in the present work was to maximize the number of states in **P** without causing absorbing states, resulting in a 24×24 matrix. For the coupling matrix **C**, the dimensions were set to 111×23, giving 111 and 23 unique values for H_s and T_p respectively. This is equal to the number of unique values in the hindcast dataset which has a resolution of 0.1 for H_s and logarithmic spacing between sampled T_p levels.

The VAR model coefficients was fitted using maximum likelihood estimation (MLE) [39] followed by assessment using the Akaike information criterion (AIC) as presented in [1]. The best fit was obtained by including the past seven values for estimating the next, i.e. p =7.

For the VARMA model another approach was chosen. AIC is applied to complete models, requiring extensive computational effort for coefficient fitting of Φ and Θ for a large set of combinations of p and q in the VARMA model. Therefore, considering the practical time constraint of design processes, the approach described given by Tiao and Tsay [33] was applied. The two-way tables of the P-values of extended cross-correlation matrices are first computed using multivariate Ljung-Box statistics of the series [34]. The selection of p and q is then taken as the combination which give the lowest P-value at a 5% significance level, MLE analysis to determine Θ and Φ. The optimal combination of p and q was found to be 2 and 3 respectively.

4. Wave model testing and benchmarking

This section presents the methodology for testing and comparing the models described in section 3.

4.1. Ship added resistance due to waves

Vessels in a seaway experience higher levels of resistance than in calm water conditions due to the exposure to waves, wind and current. These effects cause an increase in propulsion power and fuel consumption required to maintain speed. If the long-term weather models are to be applied for simulation-based design of ships, it is important that the resulting values of added resistance is representative in terms of resistance level and variation. To test these criteria, a case study is performed where we assume the following:

- **Head seas**
  Since the models do not consider wave propagation direction, constant head seas are assumed.
- **Frequency domain pressure integration**
  Added resistance levels are estimated using the pressure integration method [12].
- **Wave added resistance**
  Only the wave added resistance component is considered. This is expressed as a percentage of the calm water resistance, estimated using Holtrop's method [18].

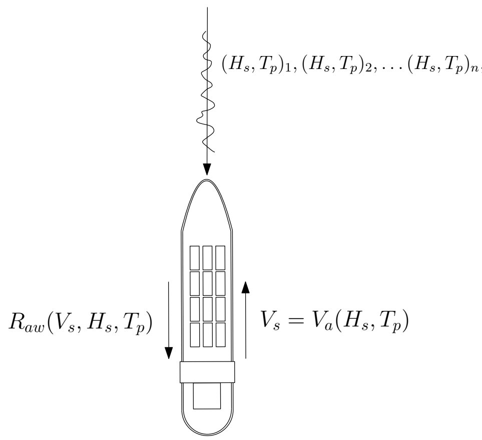

Figure 4: Added resistance analysis assumptions

Figure 4 illustrates the assumptions of the case study. The case vessel is the S175 hull, of which estimates of calm water and added wave resistance is performed in ShipX. The stochastic wave model time series is given as input, and equivalent time series of resistance is computed. To avoid unrealistic speed-sea state combinations, the attainable speed is computed as outlined in the following section.

The S-175 containership is adopted as a case vessel for the added resistance calculations. The same hull is used to obtain limiting sea state curves applied in the operability studies in Section 4.3. Vessel particulars are listed in table 1.

Table 1: Case vessel particulars S-175 containership

Parameter	**Value**
L_{pp}	175 m
Beam	25.4 m
Draft	9.5 m
GM_t	2 m
r_{44}	35 %B
r_{55}	25 %L_{pp}

4.1.1. Voluntary speed loss

In harsh conditions, the ship master may opt for reducing speed in order to save fuel and avoid large motions and loads on equipment and cargo. Finding the correct relationship between occurring sea state conditions and voluntary speed loss is difficult, as the choice and level the of speed reduction is to some extent subjective in terms of the ship master's opinion. In addition, factors like vessel and delivery schedule, as part of a larger logistical system, is likely to influence the decision. In most cases, the speed is adjusted to avoid slamming, excessive accelerations and propeller racing [25]. The vessel speed is adjusted according to the probability of these events within each occurring sea state, calculated using frequency domain short-term statistics.

Table 2: Voluntary speed loss criterion (Prpić-Oršić and Faltinsen [25])

Criterion	**Probability**	**Limit**	**Location**
Slamming	0.01	-	Bow
Deck wetness	0.05	-	Bow
Propeller emergence	0.1	-	Propeller
Vertical acceleration	-	0.215 g RMS	COG

A target transit speed of 20 knots and a lower speed threshold of 15 knots is assumed. Sea states that do not allow sailing above the lower speed threshold in compliance with the criteria in Table 2 are discarded.

4.2. Transition characteristics of H_s

Sea states develop due to two physical factors: wind and swell. Wind is caused by differences in atmospheric pressure, causing a flow of air from high-pressure to low-pressure areas. Boundary layer interaction between the air and sea surface produce waves with temporal characteristics depending on duration and wind intensity. In addition to locally wind-generated waves, waves generated elsewhere may propagate into the area, giving rise to swell. The analysis procedure presented in this section targets the periods of H_s increase and decrease with the intention of determining whether the physical process of sea state development is captured in the stochastic models.

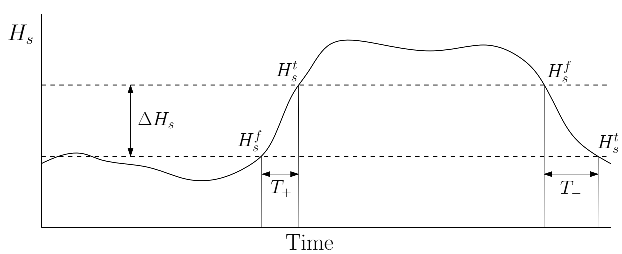

Figure 5: Analysis procedure for determination of transition periods of H_s

Figure 5 illustrates the procedure for sea state transition assessment. We define first an H_s interval of N values with constant increment λ on the form $H_s^{i=1..N}$ such that

$$\begin{aligned} \lambda &= H_s^i - H_s^{i-1}, \quad i = 2 \ldots N \\ N &= \frac{H_s^{max} - H_s^{min}}{\lambda} \end{aligned} \tag{27}$$

Since we are interested in evaluating the transition period between H_s levels, we define variables H_s^f and H_s^t corresponding to the initial and final H_s value, respectively. The corresponding difference, ΔH_s, is therefore

$$\Delta H_s = H_s^t - H_s^f \tag{28}$$

A positive ΔH_s indicates an increase in sea state energy and wave amplitudes. An observation of the period between H_s level i and j is denoted T_+^{ij} if $i > j$ and T_-^{ij} if $i < j$. Figure 6 outlines the relationship between the variables and the methodology of sorting and comparing sea state development periods.

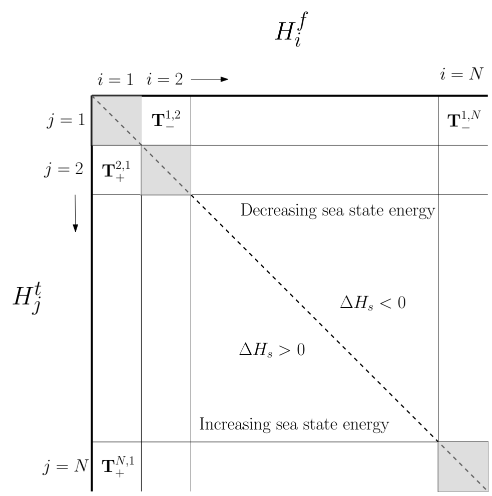

Figure 6: Relation between variables and structure of sorted transition periods

$\mathbf{T}_+^{ij}$ and $\mathbf{T}_-^{ij}$ are vectors containing all observations of periods for increasing and decreasing H_s levels from index i to j, respectively. In the present work we examine the periods of sea state development ΔH_s. H_s^f and H_s^t combinations resulting in the same ΔH_s are therefore collected in the same set of observations. Equations 29 and 30 expresses the mean increase and decrease periods for a given ΔH_s-level, denoted $\bar{T}_{\Delta H_s}^+$ and $\bar{T}_{\Delta H_s}^-$ respectively.

$$\bar{T}_{\Delta H_s}^+ = \frac{1}{n_{\Delta H_s}^+} \sum_{k=1}^{n_{\Delta H_s}^+} T_+^k, \quad H_j^t - H_i^f = \Delta H_s > 0 \tag{29}$$

$$\bar{T}_{\Delta H_s}^- = \frac{1}{n_{\Delta H_s}^-} \sum_{k=1}^{n_{\Delta H_s}^-} T_-^k, \quad H_j^t - H_i^f = \Delta H_s < 0 \tag{30}$$

We assess the occurrence of transition on the interval given in Table 3. The interval is chosen to avoid too few observations of transition between the highest and lowest H_s values. We narrow our search to only cover cases where the sea state is either decreasing or increasing throughout the period, i.e. the derivative or the H_s curve is either strictly positive or negative.

Table 3: H_s transition interval

H_s^{min}	2.0 m
H_s^{max}	5.5 m
λ	0.5 m

4.3. Operability

The long-term ability to perform weather restricted marine operations and offshore activities is commonly quantified by the operability measure. To assess the operability, operable weather window persistence is examined based on the sea state characteristics at site and operational limits. Hence, the measure is dependent on the ratio between calm water and storm state durations. Hagen et al. [16] and De Masi et al. [9] investigated the quality of Markov sea state generators for application in marine operations studies, showing good agreement for H_s persistence compared to hindcast data. In the present work, we define the operational limit as a function of H_s and T_p, assessing operability for the bivariate case.

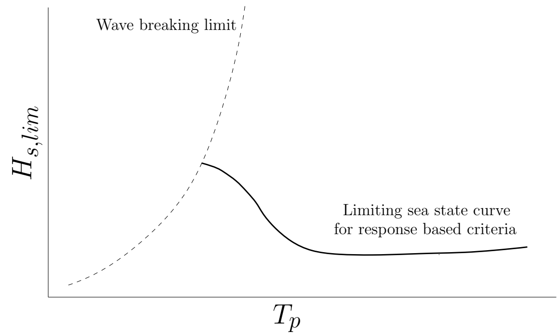

Figure 7: Limiting H_s as a function of T_p for response based criteria

Operability studies is formed around a limiting criterion which defines the border between operable and non-operable states. Response based criteria are applied as defined in [23]. Figure 7 illustrates the limiting sea state curve, which is obtained by considering the deterministic vessel response and short-term statistics using the ShipX plug-in VERES developed by SINTEF Ocean (former MARINTEK), see [14]. We assume that the operations is limited by the root-mean-square (RMS) roll response α degrees. $H^{\alpha}_{s,lim}$ is the corresponding limiting significant wave height as a function of T_p according to the curve in Figure 7.

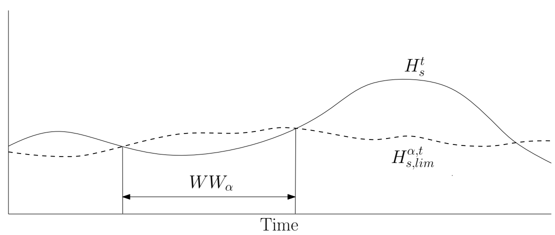

Figure 8: Weather window analysis

The bivariate time series are investigated by identifying the number and duration of operable weather windows. As illustrated in Figure 8, $H^{\alpha,t}_{s,lim}$ is computed based on the occurring T^t_p in the time series. If $H^{\alpha,t}_{s,lim} > H^t_s$, the current sea state permits operation. For operation completion, we demand a sequence of sea states to be operable. The sequence length criterion $WW_{\alpha,lim}$ is varied in order to investigate the occurrence of operable windows corresponding to different operational scenarios in the models. The operability is computed for each season s, roll limit angle α and weather window duration criterion d.

$$OP_{sd\alpha} = \frac{n_{sd\alpha}}{\lfloor \tau/d \rfloor} \times 100 \tag{31}$$

In Equation 31, $OP_{sd\alpha}$ is the percentage operability, $n_{sd\alpha}$ is the observed number of weather windows and τ is the time series length. If a weather window appears with a duration WW_α longer than the required weather window length d, the number of weather windows inside the sequence is taken as $\lfloor WW_\alpha/d \rfloor$.

5. Results

This section presents the results from the time series testing procedure given in Section 4. 10 time series spanning 25 years for each model are used in the comparison.

5.1. Sea state parameter distributions and time series correlation

The quickest and most straightforward assessment of stochastic models is done by comparing marginal distributions. Since all three models are fitted to the same hindcast dataset, one would expect the resulting output time series to be similar. Figure 9 shows the marginal distributions for the applied hindcast data, the Markov model, VAR model and VARMA model, computed using a kernel density function for each season. The irregular shape of the Markov model distribution stands out from the rest, which is caused by the finite state space assumption, see Section 3.3. The largest deviations from the hindcast distribution is also found in the Markov model, especially during winter and fall for both H_s and T_p. VAR and VARMA coincides quite well with the hindcast distributions. The largest deviations for these models are observed for the summer season for T_p.

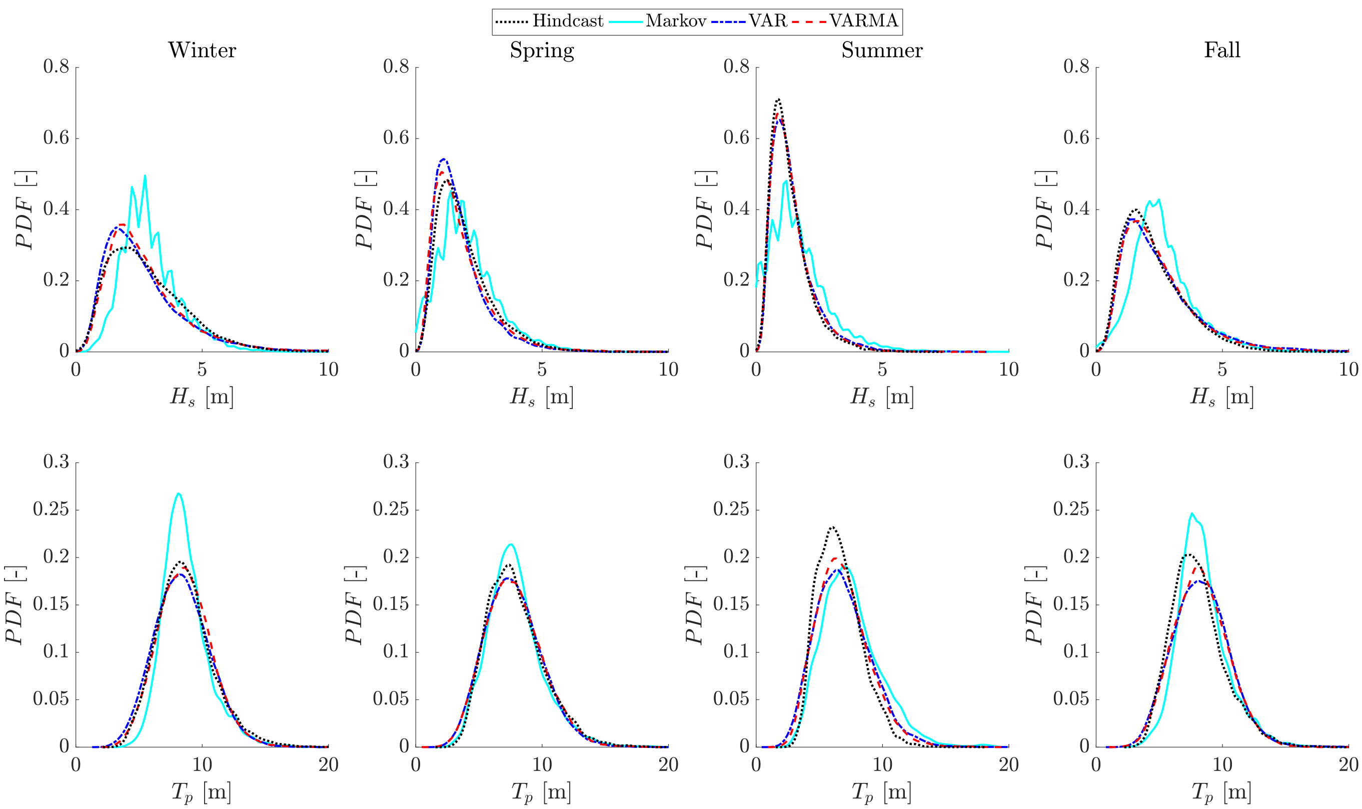

Figure 9: Marginal distributions of H_s and T_p in the hindcast and model data

Figure 10 shows scatter diagrams for the hindcast and model time series. Considering scatter shape, the Markov chain series seems to be most comparable. This is again due to the finite state space formulation, which defines clear boundaries for H_s and T_p. This assumption is not implemented in the VAR or VARMA model, which occasionally produce higher H_s values than is found in the hindcast time series. The overall scatter shape is determined by the Rosenblatt transform (see Section 3.2.1), and gives similar shape for the Markov model. Low lognormal standard deviation values for the conditional distribution of T_p produce a narrow distribution of T_p for high H_s values, clearly visible for the VAR and VARMA results.

Figure 11 shows the autocorrelation and cross-correlation functions of H_s and T_p for the hindcast dataset and models. The Markov model curves deviates significantly from the others, which can be explained by the memoryless assumption. The VAR

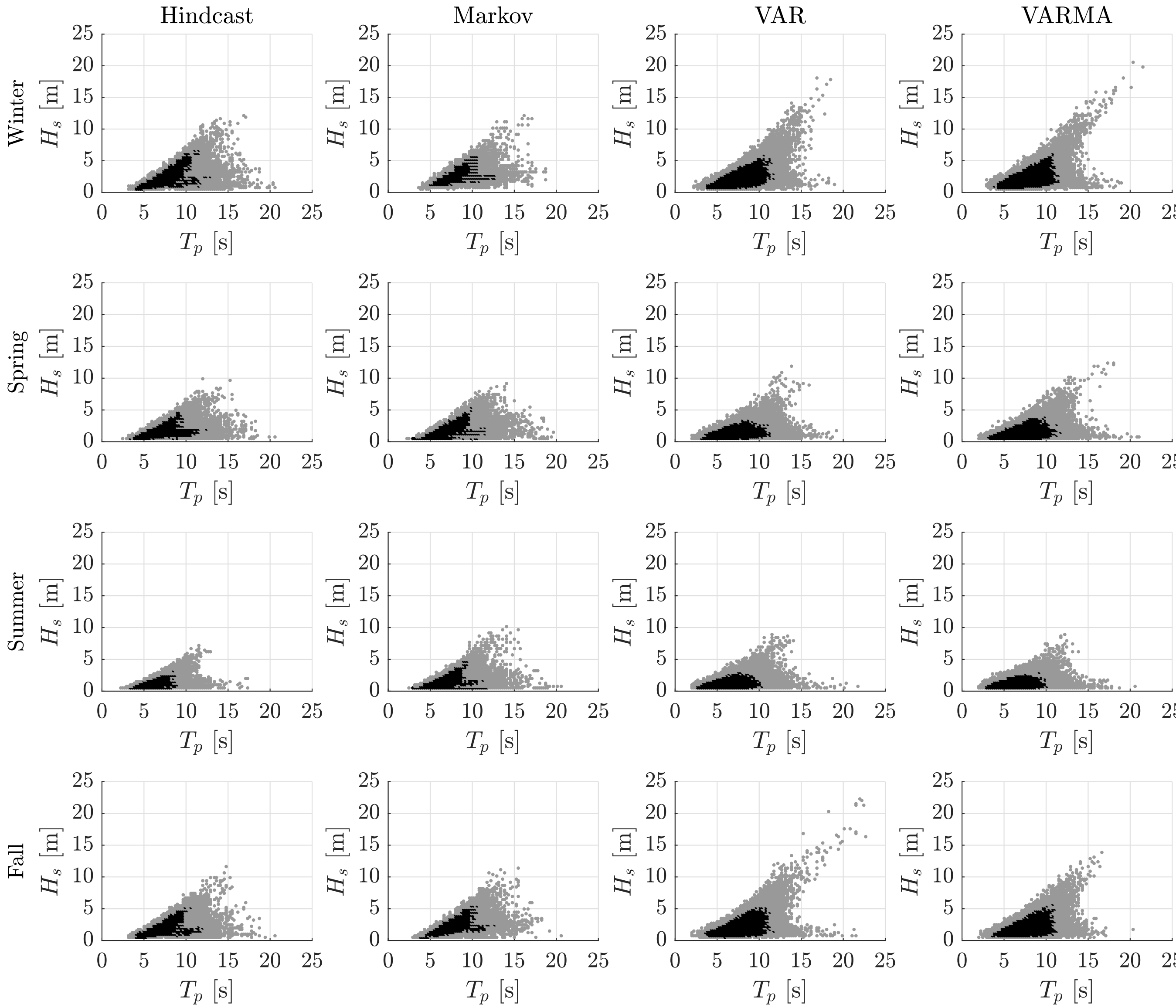

Figure 10: Scatter of hindcast and model H_s and T_p occurrences. Black areas indicate sea states with a higher number of occurrences than the average number of occurrences for all observed sea states for the given model and season.

and VARMA models agree well with the hindcast data in general, giving only minor differences in the autocorrelation function results. For the cross-correlation results the VAR model is found to overestimate slightly.

5.2. Added resistance

The added resistance results, computed using the procedure presented in Section 4.1, is given in Figure 12. Each set of time series is represented by a boxplot showing the distribution estimated added resistance fraction. In addition, an operability value is plotted showing the percentage of time the vessel was able to maintain an operable speed on the range 15-20 knots limited by the criteria in Table 2.

The distribution of added resistance is linked to the marginal distributions presented in Figure 9. However, not all sea states are included in the added resistance calculations as a result of the limiting criteria in Table 2, and the mapping from sea state intensity to added resistance is not linear. The results show that the distribution of added resistance is similar for the hindcast data and model results. Maximum observed added resistance is 60 to 75 % of the calm water resistance levels for all datasets.

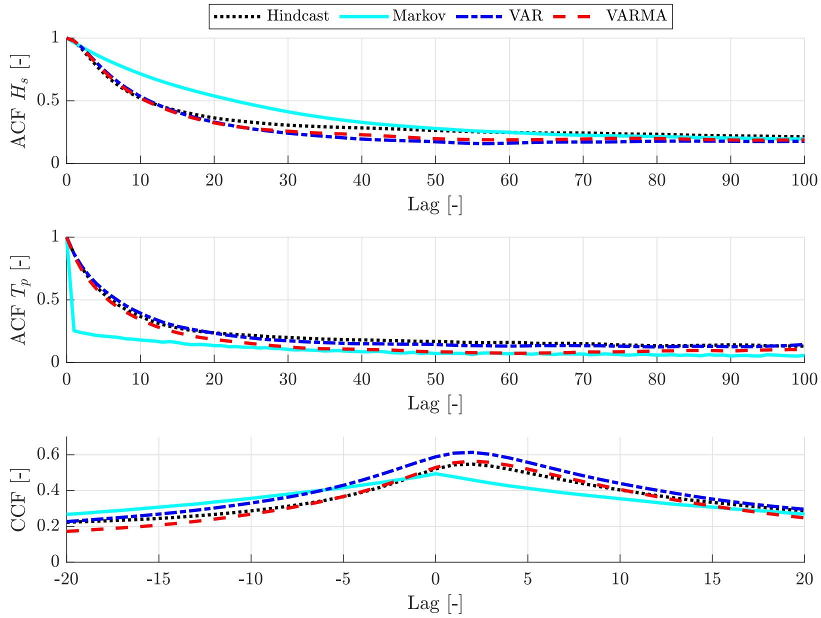

Figure 11: Autocorrelation function (ACF) and cross-correlation function (CCF) for hindcast and model H_s and T_p time series

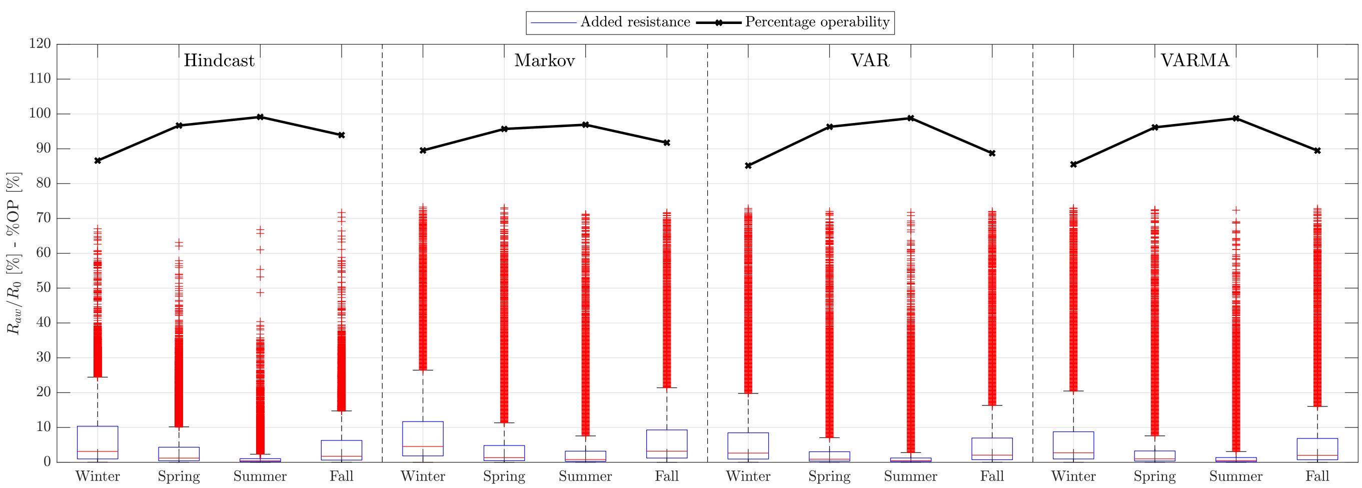

Figure 12: Added resistance estimates for speeds 15-20 knots according to attainable speed curve.

The seasonal variation does however vary significantly depending on model formulation. The top whiskers indicate that Markov results gives the highest added resistance levels for all seasons. It also produces higher estimates during fall season than the VAR and VARMA models do for winter season, which according the hindcast data is incorrect. The VAR and VARMA models are very similar, differences occur mainly in the outliers. Model seasonal percentage operability show a similar curve shape as for the hindcast data. However, the Markov model obtains a more invariable curve with respect to seasonal variation than the hindcast data. For the VAR and VARMA models the opposite is observed, underestimating the operability for the winter and fall season.

5.3. *Transition characteristics*

The marginal distributions and added resistance results shown in the previous sections addresses the occurrence of single, independent sea states. The current and following section presents results where the temporal characteristics and persistence is vital.

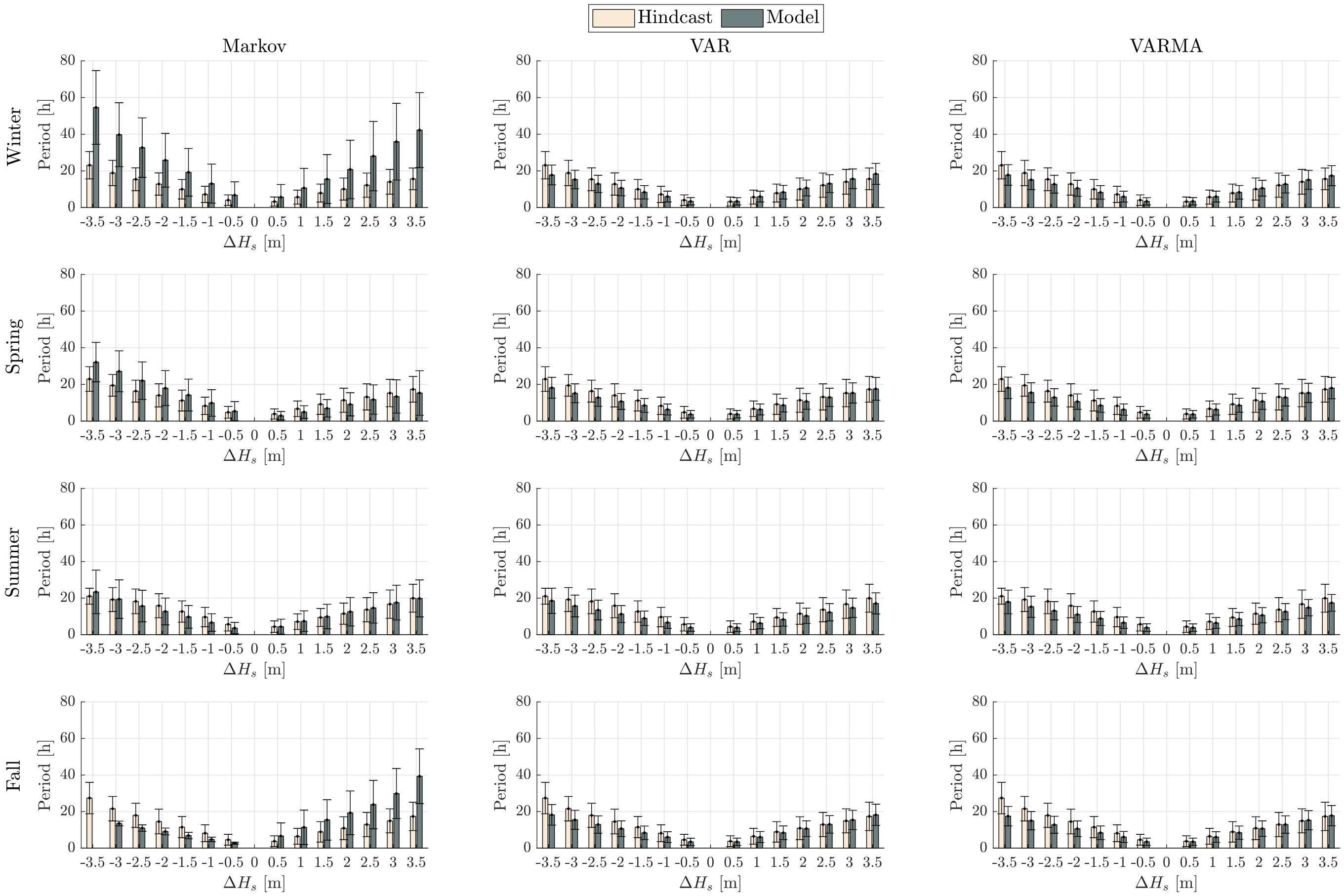

Figure 13: Transition times between sea state levels sorted according to season and model.

Figure 13 shows the results from the sea state intensity transition analysis presented in Section 4.2. Hindcast and model results is compared in each plot sorted according to model formulation and season. The hindcast data shows a gradual increase in average period from 0 to ± 3.5 m H_s. Decrease periods are slightly larger than the corresponding increase periods, which is explained by the physical process of wave excitation and dissipation. The VAR and VARMA models do not show a similar behaviour. These transition periods are more symmetrical, closely matching the increase periods of the hindcast data.

The Markov model deviates from the other results. In the winter season, the transition periods are significantly larger for both sea state energy increase and decrease compared to the other time series. The summer season is similar to the hindcast results, especially for increase periods. Spring and fall season results show a definite asymmetric behaviour with respect to increase vs. decrease periods. The spring season results indicate that an increase in H_s occurs more rapidly than the corresponding decrease of the same magnitude. The opposite is found for the fall season. This occurs as a consequence of the finite state assumption of the Markov model and the seasonal transform. As time progresses, the state levels update according to the continuous seasonal transformation presented in Section 3.2.3. During spring season, the seasonal average decreases from the harsh winter to the calm summer. This implies that for cases where the model maintains a constant state over time, a slight decrease in significant wave height is detected using the analysis procedure given in Section 4.2. Since we limit our analysis to period intervals where H_s is strictly increasing or decreasing, these small decreases affects the number and duration of observed periods. The same effect occurs during the fall season, though with an increase in seasonal average from summer to winter. Summer and winter season represents the minima and maxima in seasonal average respectively, thereby limiting this effect by consisting of both an increasing and decreasing interval of seasonal average.

Table 4: Increase and decrease period ratio. Ratios larger than 1 indicate longer increase than decrease periods.

Season	Hindcast	Markov	VAR	VARMA
Winter	0.68	0.98	1.04	0.98
Spring	0.75	0.50	0.97	0.99
Summer	0.99	0.80	0.91	0.96
Fall	0.61	2.51	1.00	1.02

To assess the symmetry of characteristic transition periods for the time series, a linear curve was fitted to the averages presented in Figure 13. The slope of the fitted curves was then taken as a basis for quantifying symmetry, noted τ_i and τ_d for increase and decrease respectively. Table 4 lists the computed curve slope ratios τ_i/τ_d. VAR and VARMA results show very symmetrical behaviour in terms of H_s increase and decrease periods, which is not consistent with the hindcast data. The effect of seasonal average on the Markov model results, as mentioned above, is visible also in the period ratios. Spring and fall season obtains a value of 0.50 and 2.51 respectively, outside the range of the other case results.

5.4. Operability

As stated in Section 4.3, the formulation of operability in this paper is dependent on the occurrence of operable weather window, defined by a limiting sea state curve and operational duration. Figure 14 shows a comparison of hindcast and model operability estimates for varying operational limit and weather window length criterion sorted according to season. The plots show constant operability lines, i.e. the contours of the operability surface, expressing how the long-term wave model formulation has affected our understanding of the vessel's capability to perform operations.

It is apparent that the Markov model performs poorly in terms of replicating weather windows. The Markov property, often referred to as the memoryless property, is evidently not suited for studies addressing events stretching over multiple time steps. Figure 11 shows that the auto- and cross-correlation is poorly replicated by the Markov model, which clearly affects the operability estimates significantly. The constant-operability curves obtain a similar shape as for the hindcast data, but the values suggests an underestimation of weather window occurrence.

The VAR and VARMA models produce similar curves in terms of curve shape and value. The difference from the hindcast data results are found to depend on season, with reasonably low differences during winter and spring, and larger differences during summer and fall.

6. Discussion

We have now covered the modelling assumptions, assessment methods and the corresponding results. This section discusses the quality of the models in the context of simulation-based design application.

6.1. Comparison methodology

In the present work, we have assessed three formulations for long-term modelling of sea states. The models produce bivariate synthetic time series of standardised wave spectrum parameters H_s and T_p. Even though the presented models are formed around statistical analyses of hindcast data, by means of correlation mapping and curve fitting, the models have been assessed

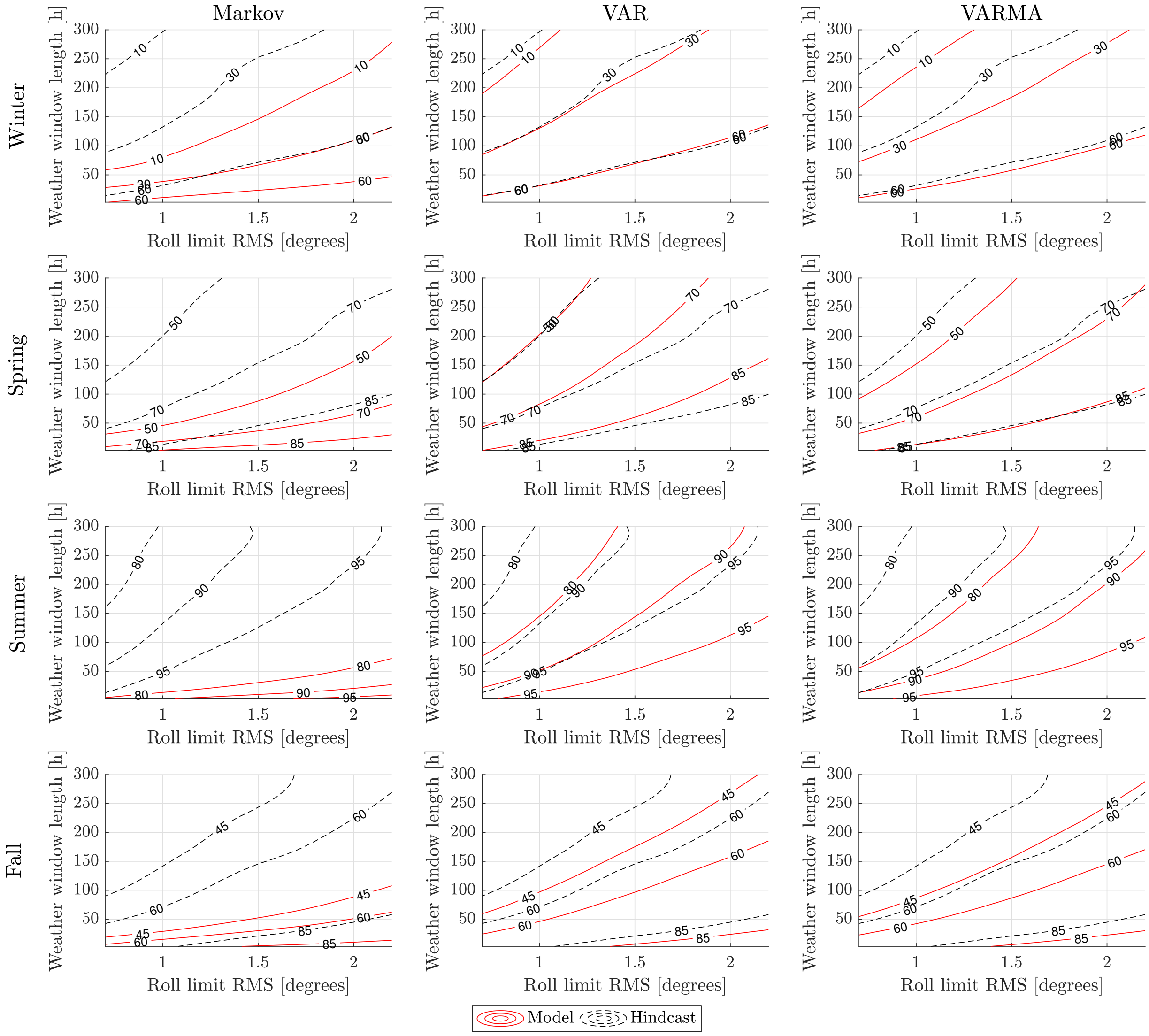

Figure 14: Operability results sorted according to model and season

in terms of the physical interpretation the output time series represents. This choice of methodology follows from our interest in the application of the models; simulation-based design of ships and ocean structures. The chosen basis of comparison, added resistance, operability and H_s transition characteristics, represents important factors in this context which incorporates the physical wave generation process and the performance of ships and marine structures.

6.2. *Model abstraction*

Vanem [35] provides good arguments for why waves should be modelled as a stochastic process, especially pointing towards the system complexity and infinite number of interrelated parameters needed to provide an exact description. The dataset used to construct the presented models is WAM10 results (see [20] and [26]), a physical model for wave-atmospheric coupling frequently used to establish wave hindcasts and forecasts. This implies that our foundation for constructing the stochastic models is resting on the modelling assumptions and uncertainties present in the WAM10 implementation. Reistad et al. [26] shows that the WAM10 results are improved compared to the frequently applied ERA-40 reanalysis. Comparison with wave buoy measurements show that H_s and mean zero upcrossing period, T_z, estimates has improved significantly with the main deviations occurring at the upper levels. Work towards improving forecasting accuracy and hindcast database quality is performed continuously. However, awareness of the fact that hindcast data is a representation of real waves, and not direct observation of the phenomenon itself, should be kept clear in mind during model development.

Assuming that the data used for model fitting is a sufficient representation of real waves, our choice of modelling formulations introduce further abstractions of the real system. This process is outlined in Figure 1, and described in detail in Section 2. The choice of time series models was Markov chains, VAR and VARMA, representing alternative specifications of the conceptual model. In addition, a seasonal transformation method is applied to model the variation of statistical parameters through the year. These assumptions is formed from wave system theories developed over years of ocean research and modelling attempts.

6.3. Application in simulation-based design

According to Monbet et al. [22], the definition of a good model involves its intended application. In the present work, we consider wave models in the context of simulation-based design, with the intention of using the models for replicating the operational environment of ships and marine structures. We have addressed three parameters which, depending on design object type and operational description, is of interest during design. Three alternative model formulations has been presented and tested with varying assumptions and fidelity levels. If we follow Bergström et al. [4], assessing fidelity level and sources of uncertainty for different models applied in simulation-based design of Arctic transport systems, the required model fidelity for application in design is that which further increase of fidelity will not influence design decisions. The results presented in the present work appears to be fall into two groups. The Markov model results does not provide a sufficient replication of H_s and T_p marginal distributions, affecting the added resistance distribution significantly. Further, the estimated operability and H_s transition characteristics, depending on the temporal development, deviates to a large degree from hindcast levels. These findings therefore disagree with the conclusions of Hagen et al. [16] and De Masi et al. [9], stating that Markov models produce similar results in terms of persistence and weather windows as for hindcast data. However, the definition of weather windows and Markov model formulation is different in the present work to that in [16] and [9]. As mentioned in Section 4.3, our study considers weather windows with an H_s threshold as a function of T_p, defined by the limiting sea state curve for the vessel. This procedure is chosen with the intention of incorporating the inherent operational limits of the vessel design, expressed using response-based criteria. In [16] and [9], the Markov model is developed with the intention of studying challenges related to marine operations, where a constant H_s limit is commonly applied [10]. Differences in state space formulation, seasonal transformation and hindcast data intensity and volatility may also affect the quality of the Markov model in terms of replicating weather windows.

The VAR and VARMA model performs more similarly. Both models coincide well with the hindcast marginal and added resistance distributions. H_s transition characteristics are found to be too symmetrical compared to hindcast data, meaning that the physical process of wave excitation and dissipation is not well represented. Weather windows are well represented during winter and spring. During summer and fall, we observe an underestimation of operability, most prominent during long weather window requirements. The testing methodology in the present work revealed only minor differences in the VAR and VARMA models. Hence, we see little benefit in constructing a VARMA model to improve the estimates of the VAR model.

A variety of model schemes and data transformations exists for stochastic time series models. In the present work, our approach is to construct models that produce the overall best results for the intended purpose, i.e. application in simulation-based design with focus on added resistance, operability and transition characteristics. This approach resulted in a different formulation for the seasonal transform for the three tested models, where the Markov and VAR model was constructed using the transform given in Equation 11 and the VARMA model using Equation 10. It should be noted that different options may produce better results in other contexts. In our opinion, a complete model follows a testing procedure with clear objectives and applicability thresholds.

The chosen wave model testing approach in the present work targets the generation of low to medium harsh sea states. We have applied a set of voluntary speed loss criteria for the added resistance analysis, and the operating limits in the operability study does not permit harsh conditions. In the scatter plot of Figure 10, it is shown that the VAR and VARMA models produce extreme sea states far outside the interval of the hindcast data. The importance and relevance for these values are however questionable for the presented application. There is no doubt that extreme sea states are of great importance for the development and operation of ships and marine structures, especially for ultimate and accidental limit state design. However, it can be argued that the design point for a ship travelling in waves in terms of e.g. installed power and hull design is well below these sea state, and that their appearance in the data has little impact on these design parameters. In a simulation model, as well as for real ships, a weather routing system will keep the ship clear of the worst storm events. Marine operations are also planned according to weather forecast to minimise the probability for harsh conditions. Extreme sea states must be taken into consideration during design of scantlings and global strength, but this subject is covered by the classification societies and government regulators during the detailed engineering phase.

Conclusion

This paper presents three bivariate stochastic long-term wave models for the North Sea as candidates for application in simulation-based design. The models are tested by analysing their effect on estimated added resistance and operability for a case vessel, and wave growth and decay periods is calculated to assess the replication of the physical wave process. Each test is performed using 10 synthetic time series of 25 years, and the results are compared towards hindcast data from 1958-2016.

The Markov model performs worst in the applied tests. Our conclusion is that the memoryless property and finite state-space formulation is not suited for constructing synthetic time series for applications covered by the presented tests.

Only small differences are detected in the test results of the VAR and VARMA models. Hence, we conclude that the VAR model gives a sufficient description of H_s and T_p in a context where extending to VARMA is a viable option. However, our results indicate that all three stochastic models produce time series where the physical wave process is not fully captured, especially for parameters stretching over multiple sea states. Application of the models should therefore follow a validity check based on the parameter of interest.

Acknowledgement

The authors are grateful for the financial support from the Research Council of Norway through the Centre for Research based Innovation (SFI) Smart Maritime project nr. 237917/O30.

Declarations of interest

None

References

[1] Akaike, H., 1973. Information Theory and an Extension of the Maximum Likelihood Principle. In: Proceedings of the Second International Symposium on Information Theory. Budapest.

[2] Anastasiou, K., Tsekos, C., 1996. Persistence statistics of marine environmental parameters from Markov theory, Part 1: Analysis in discrete time. Applied Ocean Research 18 (4), 187–199.

[3] Bergström, M., Ehlers, S., Erikstad, S. O., 2014. An approach towards the design of robust arctic maritime transport systems. Maritime-Port Technology and Development, 185–192.

[4] Bergström, M., Erikstad, S. O., Ehlers, S., 2017. The Influence of model fidelity and uncertainties in the conceptual design of Arctic maritime transport systems. Ship Technology Reasearch - Schiffstechnik 64 (1), 40–64.

[5] Bitner-Gregersen, E. M., Ewans, K. C., Johnson, M. C., aug 2014. Some uncertainties associated with wind and wave description and their importance for engineering applications. Ocean Engineering 86, 11–25.

[6] Bitner-Gregersen, E. M., Guedes Soares, C., 2007. Uncertainty of average wave steepness prediction from global wave databases. In: Proceedings of MARSTRUCT Conference. No. March. Glasgow.

[7] Box, G. E. P., Cox, D., 1964. An Analysis of Transformations. Journal of the Royal Statistical Society. Series B (Methodological) 26 (2), 211–252.
URL http://www.jstor.org/stable/2984418

[8] Campos, R., Guedes Soares, C., 2016. Comparison and assessment of three wave hindcasts in the North Atlantic Ocean. Journal of Operational Oceanography 9 (1), 26–44.

[9] De Masi, G., Bruschi, R., Drago, M., may 2015. Synthetic metocean time series generation for offshore operability and design based on multivariate Markov model. In: OCEANS 2015 - Genova. IEEE, Genova, Italy, pp. 1–6.

[10] DNV, 2011. DNV-OS-H101 - Marine Operations, General.

[11] DNV GL, 2017. DNVGL-RP-C205 - Environmental conditions and environmental loads.

[12] Faltinsen, O., Minsaas, K., Liapis, N., Skjørdal, S., 1980. Prediction of resistance and propulsion of a ship in a seaway. In: 13th Symposium on Naval Hydrodynamics. Tokyo.

[13] Fathi, D. E., Grimstad, A., Johnsen, T., P. Nowak, M., Stålhane, M., 2013. Integrated Decision Support Approach for Ship Design. In: OCEANS - MTS/IEEE. Bergen, Norway.

[14] Fathi, D. E., Hoff, J. R., 2017. ShipX Vessel Responses (VERES) Theory Manual.

[15] Guedes Soares, C., Cunha, C., 2000. Bivariate autoregressive models for the time series of significant wave height and mean period. Coastal Engineering 40 (4), 297–311.

[16] Hagen, B., Simonsen, I., Hofmann, M., Muskulus, M., 2013. A multivariate Markov weather model for O&M simulation of Offshore wind parks. Energy Procedia 35 (1876), 137–147.

[17] Hogben, N., Dacunha, N. M. C., Olliver, G. F., 1986. Global Wave Statistics. Published for British Maritime Technology by Unwin Brothers Limited.

[18] Holtrop, J., Mennen, G., 1982. An approximate power prediction method. International Shipbuilding Progress. Marine Technolgy Monthly, Rotterdam 29.

[19] Kerkhove, L. P., Vanhoucke, M., 2017. Optimised scheduling for weather sensitive offshore construction projects. Omega 66, 58–78.

[20] Komen, G. J., Cavaleri, L., Donelan, M., Hasselmann, K., Hasselmann, S., Janssen, P. A. E. M., 1994. Dynamics and Modelling of Ocean Waves. Cambridge University Press, Cambridge.
URL http://ebooks.cambridge.org/ref/id/CBO9780511628955

[21] Marzi, J., Papanikolaou, A., Corrignan, P., Zaraphonitis, G., Harries, S., 2018. HOLISTIC Ship Design for Future Waterborne Transport. In: Proceedings of the 7th Transport Research Arena TRA 2018. Vienna, Austria.

[22] Monbet, V., Ailliot, P., Prevosto, M., 2007. Survey of stochastic models for wind and sea state time series. Probabilistic Engineering Mechanics 22 (2), 113–126.

[23] NATO, 2000. STANAG 4154: Common Procedures for Seakeeping in The Ship Design Process.
URL https://standards.globalspec.com/std/113486/nato-stanag-4154

[24] Poirion, F., Puig, B., jun 2010. Simulation of non-Gaussian multivariate stationary processes. International Journal of Non-Linear Mechanics 45 (5), 587–597.

[25] Prpić-Oršić, J., Faltinsen, O. M., apr 2012. Estimation of ship speed loss and associated CO2 emissions in a seaway. Ocean Engineering 44, 1–10.

[26] Reistad, M., Breivik, Ø., Haakenstad, H., Aarnes, O. J., Furevik, B. R., Bidlot, J. R., 2011. A high-resolution hindcast of wind and waves for the North Sea, the Norwegian Sea, and the Barents Sea. Journal of Geophysical Research: Oceans 116 (5), 1–18.

[27] Sargent, R. G., 2013. Verification and validation of simulation models. Journal of Simulation 7 (1), 12–24.

[28] Shyshou, A., Gribkovskaia, I., Barceló, J., 2010. A simulation study of the fleet sizing problem arising in offshore anchor handling operations. European Journal of Operational Research 203 (1), 230–240.

[29] Skjong, S., Rindarøy, M., Kyllingstad, L. T., Æsøy, V., Pedersen, E., 2017. Virtual prototyping of maritime systems and operations: applications of distributed co-simulations. Journal of Marine Science and Technology, 1–19.

[30] Stefanakos, C. N., Athanassoulis, G., 2003. Bivariate Stochastic Simulation Based on Nonstationary Time Series Modelling. In: Proceedings of the 13th International Offshore and Polar Engineering Conference. Vol. 5. pp. 46–50.

[31] Stefanakos, C. N., Athanassoulis, G. A., 2001. A unified methodology for the analysis, completion and simulation of nonstationary time series with missing values, with application to wave data. Applied Ocean Research 23 (4), 207–220.

[32] Stefanakos, C. N., Belibassakis, K. A., 2005. Nonstationary Stochastic Modelling of Multivariate Long-Term Wind and Wave Data. In: 24th International Conference on Offshore Mechanics and Arctic Engineering: Volume 2. ASME, pp. 225–234.

[33] Tiao, G. C., Tsay, R. S., jan 1983. Multiple Time Series Modeling and Extended Sample Cross-Correlations. Journal of Business & Economic Statistics 1 (1), 43–56.

[34] Tsay, R. S., 2014. Multivariate Time Series Analysis: With R and Financial Applications. Wiley.

[35] Vanem, E., feb 2011. Long-term time-dependent stochastic modelling of extreme waves. Stochastic Environmental Research and Risk Assessment 25 (2), 185–209.

[36] Vernengo, G., Gaggero, T., Rizzuto, E., 2016. Simulation based design of a fleet of ships under power and capacity variations. Applied Ocean Research 61, 1–15.
URL http://dx.doi.org/10.1016/j.apor.2016.09.003

[37] Vernengo, G., Rizzuto, E., 2014. Ship synthesis model for the preliminary design of a fleet of compressed natural gas carriers. Ocean Engineering 89, 189–199.

[38] WAMDI Group, dec 1988. The WAM Model - A Third Generation Ocean Wave Prediction Model. Journal of Physical Oceanography 18 (12), 1775–1810.

[39] Wei, W. W., 1990. Time series analysis: Univariate and multivariate models. Addison-Wesley.